Annals of Pharmacy Practice and Pharmacotherapy
ISSN: 3062-4436
2025, Volume 5, Issue 2, Page No: 45-58

Available online at: www.galaxypub.co/page/journals

Galaxy Publication

Toward Individualized Lymphodepletion: Development of a Population Pharmacokinetic Model of Fludarabine in Patients Undergoing CAR T-Cell Therapy

Lucas Meyer[1]*, Anna Schmid[2], Stefan Braun[1]

[1]Department of Clinical Pharmacy and Medication Therapy, Faculty of Pharmaceutical Sciences, ETH Zurich, Zurich, Switzerland
[2]Department of Pharmacotherapy and Patient Care, Faculty of Medicine, University of Bern, Bern, Switzerland.

***E-mail** ✉ lucas.meyer@gmail.com

Received: 24 April 2025; **Revised:** 03 August 2025; **Accepted:** 06 August 2025

ABSTRACT

Population pharmacokinetic (popPK)-guided dosing of fludarabine in conditioning regimens has been shown to influence clinical outcomes in hematopoietic stem cell transplantation. However, no popPK model has yet been specifically developed for patients receiving fludarabine as part of lymphodepletion before chimeric antigen receptor (CAR) T-cell therapy. The present study aimed to establish a population pharmacokinetic model of fludarabine in this setting. This prospective study was carried out at a tertiary care hospital between January 2021 and July 2022. Demographic, clinical, and laboratory data were collected for all participants. Blood samples were obtained on days 1 and 3 of the lymphodepleting regimen at multiple post-dose time points (1.5, 2, 7, and 24 hours) and immediately before CAR T-cell infusion. Plasma concentrations of fludarabine were quantified using an ultra-performance liquid chromatography–tandem mass spectrometry method following liquid–liquid extraction. Population pharmacokinetic analysis was conducted using nonlinear mixed-effects modeling (NONMEM). A total of 56 patients (59% male) with a median age of 59 years (range 23–82) were included, all treated with CAR T-cell therapy for relapsed or refractory large B-cell lymphoma. Among them, 68% received axicabtagene ciloleucel and 32% received tisagenlecleucel. In total, 348 concentration samples were available for model development. The data were best described by a three-compartment model with first-order elimination. Body weight, when scaled allometrically, was identified as a significant determinant of all pharmacokinetic parameters ($P < 0.05$). In addition, estimated glomerular filtration rate (eGFR) and the type of CAR T-cell product were significantly associated with drug clearance ($P < 0.05$), which was modeled as a combination of renal and non-renal pathways. The estimated volumes of distribution for the central, shallow peripheral, and deep peripheral compartments (V1, V2, V3) were 41.2 L, 14.5 L, and 10.8 L, respectively. Overall, body weight, renal function, and CAR T-cell product type were identified as key factors influencing fludarabine pharmacokinetics. These findings support the potential use of this model to guide individualized lymphodepletion strategies, aiming to improve efficacy while reducing treatment-related toxicity.

Keywords: Population pharmacokinetic model, Pharmacokinetics, Fludarabine, Non-Hodgkin Lymphoma

How to Cite This Article: Meyer L, Schmid A, Braun S. Toward Individualized Lymphodepletion: Development of a Population Pharmacokinetic Model of Fludarabine in Patients Undergoing CAR T-Cell Therapy. Ann Pharm Pract Pharmacother. 2025;5(2):45-58. https://doi.org/10.51847/zNUVI5FBN6

Introduction

Diffuse large B-cell lymphoma (DLBCL) is the most frequent subtype of non-Hodgkin lymphoma. Standard first-line therapy is based on chemoimmunotherapy with rituximab, which achieves durable responses in approximately 60–70% of patients [1]. Patients with relapsed or refractory disease require more intensive approaches, including high-dose chemotherapy followed by autologous stem cell transplantation and chimeric antigen receptor T-cell (CAR-T) therapy [2].

CAR-T therapy has significantly improved outcomes in relapsed/refractory lymphoid malignancies. Axicabtagene ciloleucel, tisagenlecleucel, and lisocabtagene maraleucel are approved for DLBCL after at least two prior lines

of therapy [3-5]. In addition, axi-cel and liso-cel are approved as second-line treatments for patients with early disease progression within 12 months of first-line immunochemotherapy.

Lymphodepleting chemotherapy administered before CAR T-cell infusion represents a critical preparatory phase that optimizes CAR T-cell expansion and persistence. This preparative regimen enhances therapeutic conditions by reducing endogenous immune cell populations, including T, B, natural killer (NK), and regulatory T cells, while also reshaping the tumor microenvironment by modulating pathways such as indoleamine 2,3-dioxygenase activity and upregulating costimulatory signals [6].

Beyond immune cell depletion, lymphodepletion also mitigates host immune recognition of murine-derived single-chain variable fragment CAR constructs, thereby reducing anti-CAR immune responses. The incorporation of fludarabine into conditioning regimens has been associated with improved CAR T-cell expansion and persistence, more favorable cytokine dynamics, and enhanced event-free survival in patients with non-Hodgkin lymphoma. These effects are thought to result from reduced host immune competition together with increased levels of proinflammatory cytokines, including interleukin-6, interferon-γ, and tumor necrosis factor-α, which contribute to both CAR T-cell activation and cytokine-mediated toxicity [7].

Although alternative agents such as bendamustine have shown outcomes comparable to those of fludarabine and cyclophosphamide in retrospective analyses, the combination of fludarabine and cyclophosphamide remains the standard lymphodepleting regimen in current clinical practice [8].

Fludarabine is a purine nucleoside analog administered intravenously as the prodrug fludarabine phosphate (F-ara-AMP). After administration, it is rapidly and almost completely converted to the circulating metabolite F-ara-A, which subsequently distributes into cells [9]. Inside the cell, sequential phosphorylation leads to the formation of the active triphosphate form (F-ara-ATP), which mediates its pharmacological activity by inhibiting DNA and RNA synthesis. A substantial fraction of the administered dose (approximately 40%–60%) is excreted in urine as F-ara-A within 24 hours, indicating that renal elimination is a major clearance pathway [10, 11].

Interpatient variability in fludarabine exposure highlights the need for individualized dosing strategies. This has been particularly demonstrated in hematopoietic stem cell transplantation settings, where fludarabine exposure has been linked to treatment-related mortality independent of renal function alone [12, 13]. The pharmacokinetic model proposed by Langenhorst *et al.* [14] has further shown that achieving target exposure levels is associated with improved outcomes such as leukemia-free survival and reduced relapse rates in both B-cell acute lymphoblastic leukemia and aggressive B-cell non-Hodgkin lymphoma treated with CAR T-cell therapy [15, 16]. Nevertheless, important differences exist between the population used to develop the original model and adult patients currently receiving CAR T-cell therapy, including disease burden, inflammatory status, treatment history, prior transplantation, dosing variability, and renal function variability. These differences emphasize the necessity for a dedicated population pharmacokinetic model tailored to CAR T-cell therapy settings.

Accordingly, the objective of this study was to construct a population pharmacokinetic model of fludarabine in adult patients receiving lymphodepleting chemotherapy before CAR T-cell infusion, to better characterize its pharmacokinetics in this specific clinical context.

Materials and Methods

Study design

A prospective, single-center observational investigation was conducted in adult individuals (≥ 18 years) diagnosed with relapsed or refractory large B-cell lymphoma who were scheduled to receive fludarabine-containing lymphodepleting chemotherapy before CAR T-cell therapy (axicabtagene ciloleucel or tisagenlecleucel) following at least 2 prior systemic treatment lines. The study was conducted in the Hematology Department of Hospital Universitari Vall d'Hebron (Barcelona, Spain). Ethical authorization was obtained from the institutional Clinical Research Ethics Committee (IP17/2020-PR(AG)682/2020), and all enrolled patients provided written informed consent.

Fludarabine dosing

All participants received fludarabine as a 30-minute intravenous infusion according to the assigned lymphodepletion protocol. Patients treated with axi-cel received fludarabine phosphate at 30 mg/m², together with cyclophosphamide at 500 mg/m², on days −5, −4, and −3 before CAR T-cell infusion, as per the product labeling

recommendations [3]. In contrast, those receiving tisa-cel were administered fludarabine phosphate 25 mg/m² combined with cyclophosphamide 250 mg/m² on the same schedule before infusion [4].
Since fludarabine is given as the monophosphate form (F-ara-AMP), administered doses were converted to the active metabolite equivalent (F-ara-A) using a molecular weight correction factor of 0.78.
Patients presenting with reduced renal function at the start of lymphodepleting chemotherapy were administered adjusted fludarabine doses. Based on the product information [17], dose reduction of up to 50% is recommended when creatinine clearance is between 30 and 70 mL/min, alongside close monitoring of hematologic toxicity. As precise adjustment thresholds were not fully defined, an institutional dosing algorithm was implemented. Accordingly, a 25% dose reduction was applied to patients with estimated glomerular filtration rate (eGFR) of 45–60 mL/min (Cockcroft–Gault), while a 40% reduction was applied to those with eGFR of 30–45 mL/min [18]. Cyclophosphamide dosing was maintained without modification in all cases.

Subjects

Study eligibility included adult patients (≥ 18 years) with relapsed or refractory LBCL who had previously received at least two systemic treatment lines. Patients were required to undergo fludarabine-containing lymphodepletion before infusion of commercial CAR T-cell products (axicabtagene ciloleucel or tisagenlecleucel) and to have at least one quantifiable serum fludarabine concentration available for analysis.
Clinical and demographic data collected included age, sex, anthropometric measures (weight, height, BSA, BMI), lymphoma diagnosis and date of diagnosis, prior hematopoietic stem cell transplantation with corresponding dates, ECOG performance status, and hospitalization information related to CAR T-cell therapy (admission and discharge dates). Treatment-related information was also recorded, including the start date of lymphodepletion, daily fludarabine and cyclophosphamide doses during the three-day regimen, the date of CAR T infusion, the CAR construct type, the number of prior treatment lines, and the use of bridging therapy.
Laboratory assessments comprised hemoglobin, lymphocyte count, albumin, serum creatinine, and LDH measured on days 1 and 3 of lymphodepletion and before CAR T infusion. Renal function was estimated using creatinine clearance calculated with the Cockcroft–Gault formula, according to the Spanish Society of Nephrology guidelines [19]. It was assessed at baseline and before the third dose of fludarabine.

Blood sampling collection

Outpatient sampling was scheduled according to the limited sampling model (LSM) proposed by Mohanan *et al.* [20], which identified 1, 2, 7, and 24 hours post-infusion as optimal time points balancing bias and variability. After adaptation of this approach to routine hospital practice, fludarabine concentrations were determined using samples collected at 1.5, 2, and 24 hours after infusion on days 1 and 3 of lymphodepletion, as well as 30 minutes before CAR T-cell administration. When patients remained hospitalized during the conditioning period, an additional 7-hour sample was also obtained.
Blood samples were collected in serum separator tubes containing gel, centrifuged at 2000× g for 10 minutes, and the resulting serum was divided into two aliquots. Samples were subsequently stored at −80 °C until analysis.

Analytical determination

For LC–MS/MS, analytical-grade acetonitrile (Fisher Scientific, Waltham, MA, USA) and a 5 M ammonium acetate solution (Sigma–Aldrich, St. Louis, MO, USA) were employed. A Milli-Q water purification system (Millipore, Milford, MA, USA) supplied the ultrapure water used in all experiments. Toronto Research Chemicals, Inc. (North York, ON, Canada) provided the reference materials, including fludarabine and the internal standard 2-chloroadenosine.
Measuring fludarabine levels required two sequential steps. To begin, calibration standards and QC samples were created by adding 5 µL of various working solutions to 95 µL of blank serum. This approach generated seven calibrator concentrations ranging from 1 to 1000 ng/mL, along with QC samples at three levels: 2.5 ng/mL (low), 250 ng/mL (medium), and 1000 ng/mL (high). A serum blank (no analyte added) was also included to verify method selectivity.
During extraction, 100 µL of serum taken from study samples, calibrators, or QC materials was combined with 200 µL of a chilled methanol solution (−20 °C) containing 10 ng/mL of the internal standard (2-chloroadenosine). After thorough mixing in a vortex, the mixture was centrifuged, and 90 µL of the supernatant was transferred to a new container. This was then mixed with an identical volume of a diluent made from 1 mM ammonium acetate

dissolved in a 95:5 water–acetonitrile blend (v/v). Following a brief vortex step, the final preparations were kept refrigerated at 4 °C pending LC–MS/MS injection.

A Waters Acquity UPLC system combined with an Xevo TQ MS detector (Waters Corporation, Milford). Analytical separation and quantification were performed on a Waters Acquity UPLC system interfaced with an Xevo TQ MS detector. Each run involved injecting 5 µL of either calibration or quality control solution onto a reversed-phase Acquity UPLC HSS C18 column (2.1 × 100 mm, 1.8 µm particle size; Waters, USA) at 40 °C.

Compound separation relied on a binary elution system composed of aqueous ammonium acetate (1 mM, mobile phase A) and acetonitrile (mobile phase B). The gradient was programmed to start with a low organic proportion (5% B for the first minute), then increase gradually to 30% B over the next 2 minutes. Subsequently, the organic phase was raised to 90% over 3.0 to 3.5 minutes and maintained briefly before returning to the initial conditions for column re-equilibration. The full analytical cycle lasted 5.6 minutes with a constant flow of 0.3 mL/min.

Detection was performed by electrospray ionization in positive mode, with multiple reaction monitoring (MRM) for selectivity. The monitored ion transitions were m/z 286.10 → 154.00 for fludarabine and m/z 302.00 → 170.00 for the internal standard. To ensure analytical reliability, blank injections were used to assess potential carryover after the highest concentration standard, and matrix-related interference was controlled using matrix-matched calibration and internal standard normalization.

Method performance was validated in accordance with EMA/ICH M10 guidelines [21], including linearity, precision, and accuracy. The calibration model showed strong linear behavior over the range of 1–1000 ng/mL ($R^2 = 0.999$). At the lower limit of quantification (1 ng/mL), intra-batch precision ranged from 14.3% to 18.5% CV with accuracy between −0.7% and 13.4%. For QC levels spanning 2.5 to 1000 ng/mL, intra-day precision ranged from 2.8% to 9.6% CV, and accuracy ranged from −11.9% to 12.8%. Inter-day performance at the LLOQ showed 18.2% CV and 4.2% relative error, while QC inter-day variability ranged from 6.8% to 8.0% CV with accuracy between −5.3% and 6.9%, all within acceptable regulatory limits.

Signal processing was performed using MassLynx software (v4.2 SCN 1014; Waters, USA). Concentrations were derived from calibration curves constructed by weighted (1/x) linear regression based on analyte-to-internal standard peak area ratios.

MA (USA) was used to quantify fludarabine.

Population pharmacokinetics analysis

Nonlinear mixed-effects modeling was implemented to construct the population pharmacokinetic (PopPK) model using the first-order conditional estimation method with interaction (FOCEI) in NONMEM® (v7.4.3; Icon Development Solutions, Ellicott City, MD, USA) [22]. Post-processing of model outputs, generation of goodness-of-fit diagnostics, and model evaluation were performed using Perl-speaks-NONMEM (PsN® v5.3.0) [23] together with R software (v4.2.3) [24]. Additional reporting outputs, including summary tables, were produced using Piraña (v11.1) [25].

Interindividual variability (IIV) was incorporated using an exponential error model, assuming a log-normal distribution for all pharmacokinetic parameters exhibiting variability. For analysis purposes, concentration and model data were log-transformed.

Model selection was guided by statistical and parameter-based criteria. Competing models were compared using the change in objective function value (OFV), defined as −2 log-likelihood (−2LL). For nested models differing by one parameter, decreases in OFV of 3.84 and 6.61 were considered indicative of significance at the 5% and 1% levels, respectively. In addition, parameter precision was assessed using relative standard error (RSE%), calculated as the standard error divided by the parameter estimate and expressed as a percentage.

Model development proceeded in three sequential stages. First, a structural base model was established to adequately describe the observed data. Second, potential covariate effects on pharmacokinetic parameters were systematically evaluated. Finally, the selected model was confirmed using simulation-based diagnostic tools.

Base population model

Serum pharmacokinetics of fludarabine were described using compartmental approaches expressed in terms of apparent distribution volumes, inter-compartmental clearances, and systemic elimination clearance. The potential presence of nonlinear behavior in both distribution and elimination processes was also evaluated and tested within the modeling framework.

Model adequacy was assessed through diagnostic evaluations to determine whether the structural assumptions were consistent with the observed concentration data. During this stage, correlations between random effects (non-zero covariance terms in the variance–covariance matrix) and inter-occasion variability were additionally examined as part of model refinement.
Several residual error structures were compared, including additive, proportional, and combined models on a log-transformed scale, with the final selection based on overall model fit and diagnostic performance.

Covariate selection
Covariate selection was carried out using a stepwise covariate modeling (SCM) procedure [22], in which potential predictors were evaluated sequentially. In the forward inclusion stage, covariates were added to the model if they met the 5% significance level ($P < 0.05$). This was followed by a backward elimination step, in which variables were retained only if they satisfied a stricter criterion of 1% ($P < 0.01$). In addition to statistical significance, physiological plausibility and adequate representation of each covariate within the study population were also considered to support robust model development. Time-dependent covariates were initially standardized by dividing each value by its corresponding median. Continuous covariates were incorporated into the population model after normalization using the median of the study cohort. Categorical variables were evaluated as relative (proportional) effects compared with a predefined reference category.
The influence of body weight (WGT) was assessed using power-based relationships, applying both estimated scaling exponents and fixed allometric exponents as described in previous approaches [26].

Model evaluation
Model evaluation was performed using simulation-based diagnostic methods, specifically the prediction-corrected visual predictive check (pcVPC) [27, 28]. To implement this approach, 1000 replicate datasets with identical design characteristics to those of the original data were generated from the final model. For each simulated dataset, concentration–time data were stratified into time intervals, and the 2.5th, 50th, and 97.5th percentiles were calculated within each bin. The corresponding 95% prediction intervals for these percentiles were then derived and plotted together with the observed data for comparison.
In addition, the potential clinical relevance of selected covariates was assessed using graphical exploration. Standard goodness-of-fit plots and diagnostics of the empirical Bayes estimates (ETA distributions) were also generated to further evaluate model performance.

Results and Discussion

Patient characteristics
Sixty patients were initially recruited, of whom 56 were ultimately included in the analysis. Four individuals were excluded because the fludarabine lymphodepletion protocol was not fully completed: one patient died due to septic shock, one discontinued treatment following rapid disease progression, and two experienced fever leading to delays in the conditioning regimen.
Within the analyzed cohort, 33 patients (59%) were male, with a median age of 59 years (range: 23–82). At baseline, the mean body weight was 79.6 kg (SD 12.9), and obesity (BMI > 30) was observed in two cases. Regarding CAR T-cell products, 38 patients (68%) received axicabtagene ciloleucel, whereas 18 (32%) received tisagenlecleucel. The corresponding cumulative fludarabine doses were 90 mg/m² for the axi-cel group and 75 mg/m² for the tisa-cel group, in accordance with manufacturer recommendations.
Dose reductions due to impaired renal function were implemented in six patients (two in the axi-cel group and four in the tisa-cel group). A summary of baseline demographic and clinical characteristics is provided in **Table 1.**

Table 1. A summary of baseline demographic and clinical characteristics.

Variables	Study population (n = 56)
Male sex, n (%)	33 (59)
Age; median (range)	59 (23–82)
Weight (kg)	
Mean (SD)	79.6 (12.9)

Median (range)	82.5 (52–101)
Body mass index (kg/m^2)	
Mean (SD)	25.2 (3.5)
Median (range)	25.3 (18.0–36.2)
CAR-T construct; n (%)	
Axi-cel	38 (68)
Tisa-cel	18 (32)
Histological diagnosis; n (%)	
Diffuse large B-cell lymphoma	30 (54)
Transformed from indolent lymphoma	20 (36)
High-grade B-cell lymphoma	3 (5)
Other *	3 (5)
ECOG; n (%)	
0	32 (57)
1	20 (36)
2	4 (7)
Prior lines of treatment; n (%)	
2	45 (80)
≥3	11 (20)
Prior HSCT; n (%)	21 (37)
Serum Albumin (g/dL)	
Median (range)	4 (2.7–4.8)
Renal Function [eGFR: mL/min/1.73 m^2]	
Mean (range)	90 (39.0–213.9)

* Other: T-cell/histiocyte-rich large B-cell lymphoma and intravascular large B-cell lymphoma are included in this category.Abbreviations: CAR-T refers to chimeric antigen receptor T-cell therapy; ECOG denotes Eastern Cooperative Oncology Group performance status; HSCT stands for hematopoietic stem cell transplantation; eGFR indicates estimated glomerular filtration rate.

Samples

A total of 168 fludarabine dosing events were documented, yielding 400 collected blood samples. After data screening, 348 samples were retained for pharmacokinetic modeling. At the same time, measurements below the lower limit of quantification or exceeding the upper quantification limit (and not amenable to further dilution) were excluded from the analysis set. The included concentration–time dataset consisted of 99 samples obtained at 1.5 h, 97 at 2 h, 94 at 24 h, and 51 collected 30 minutes before CAR T-cell infusion. In addition, only a limited number of samples (n = 7) were available at the 7-hour post-infusion time point. Each participant contributed a median of six samples [1-9].

Figure 1 illustrates the overall fludarabine concentration–time profiles. Each open circle denotes an individual observed serum concentration, while the connecting solid lines depict linear interpolation between consecutive sampling points.

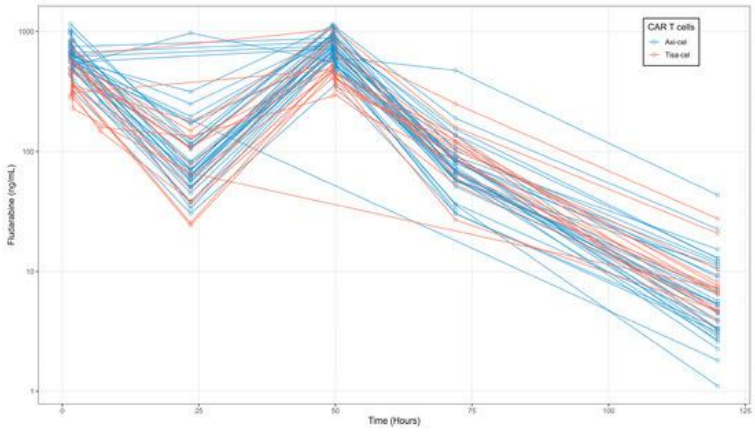

Figure 1. Plasma concentration–time profiles of fludarabine after the initial intravenous administration. Individual observed concentrations are shown as open circles, while solid lines depict linear interpolation between successive sampling points.

Population PK modeling

A three-compartment structural model most appropriately characterized fludarabine serum concentrations. The disposition model included a central compartment (V1), a shallow peripheral compartment (V2), a deep peripheral compartment (V3), and systemic clearance (CL). Drug exchange between compartments was governed by inter-compartmental clearances from V1 to V2 (CLD2) and from V1 to V3 (CLD3). This configuration improved the description of the full concentration–time course, particularly in the terminal phase, where simpler structural models showed clear systematic bias.

Interindividual variability was implemented only for CL and V1. The associated shrinkage values were low (8.9% for CL and 18.3% for V1), indicating that the data contained sufficient information to support reliable individual parameter estimation. Covariate analysis identified body weight (WGT), estimated glomerular filtration rate (eGFR), and CAR-T product type (axi-cel versus tisa-cel) as significant determinants of clearance.

Both clearance estimates across CAR-T constructs and the central volume parameter (V1) were highly precise, with relative standard errors below 10%, supporting model stability. A block structure was used to model interindividual variability in CL and V1, allowing their joint estimation and accounting for their correlation. This analysis revealed a strong positive relationship between the two parameters at the population level (correlation coefficient $\rho \approx 0.9$).

In contrast, interindividual variability for V2, V3, CLD2, and CLD3 was not incorporated due to limited data support and the inability to obtain stable or precise estimates for these parameters. This was further constrained by sparse sampling in the distribution phases, particularly for the deep compartment. Final parameter estimates are summarized in **Table 2.** Model evaluation results, including goodness-of-fit diagnostics and ETA distribution plots, are presented in **Figure 2**, with no relevant bias observed.

$$
\begin{aligned}
&CL = [CL_{non\text{-}renal} + CL_{renal}] \times f(WGT) \\
&CL_{non\text{-}renal} \begin{cases} \theta_{CAR-T1}, & \text{axi-cel} \\ \theta_{CAR-T2}, & \text{tisa-cel} \end{cases} \\
&CL_{renal} = \theta_{CRCL} \times \frac{CRCL}{96} \\
&f(WGT) = \left(\frac{WGT}{70}\right)^{3/4}, g(WGT) = \frac{WGT}{70}
\end{aligned}
\qquad (1)
$$

WGT = Weight

Between-subject variability (IIV) is presented as a percentage coefficient of variation (%CV), computed as $\sqrt{(e^{\wedge}\omega^2 - 1)} \times 100$, where ω^2 denotes the variance of the random-effect terms. A correlation value of 0.9 was estimated between the random effects.

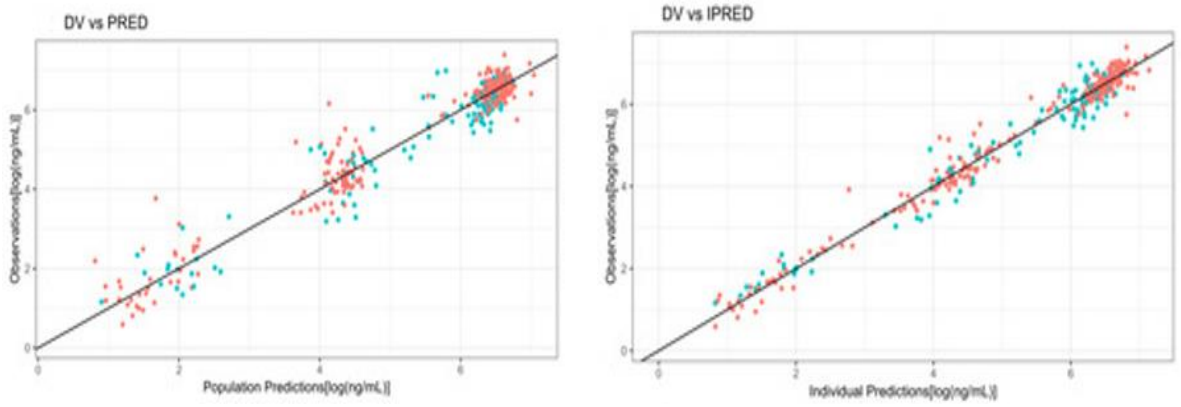

a) b)

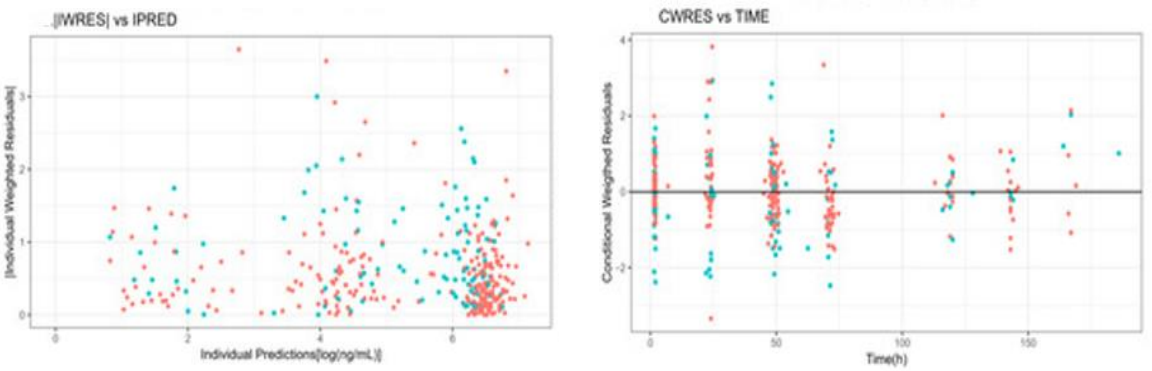

c) d)

Figure 2. Diagnostic plots for model goodness-of-fit. Blue symbols: Axi-cel; red symbols: Tisa-cel. DV, observed values; PRED, population-predicted concentrations; IPRED, individual-predicted concentrations; |IWRES|, absolute individual weighted residuals; CWRES, conditional weighted residuals. The solid line represents the line of unity.

Table 2. Final estimates of population pharmacokinetic parameters.

Parameter	Description	Estimates (RSE%)	Shrinkage (%)
CL (L/h)	$[\theta_{(CAR\_T)} + \theta_{CRCL} \times CRCL/96] \times f(WGT)$	$\theta CART$=1 = 4.4 (1.2)	-
		$\theta CART$ =2 = 3.9 (0.9)	
		$\theta CRCL$ = 1.7 (1.0)	
V1 (L)	$\theta V1 \times g(WGT)$	$\theta V1$ = 41.2 (9.3)	
V2 (L)	$\theta V2 \times g(WGT)$	$\theta V2$ = 14.5 (14.0)	-
V3 (L)	$\theta V3 \times g(WGT)$	$\theta V3$ = 10.8 (3.0)	-
CLD2 (L/h)	$\theta CLD2 \times f(WGT)$	4.8 (5.3)	-
CLD3 (L/h)	$\theta CLD3 \times f(WGT)$	3.6 (0.1)	-
IIV on CL (%)	-	29.8 (25.1)	8.9
IIV on V1 (%)	-	34.8 (3.6)	18.3
Error [log(ng/mL)]	-	0.29 (18.6)	12.1

Total plasma clearance is denoted as CL. The terms V1, V2, and V3 represent the apparent volumes of distribution for the central, first peripheral (shallow), and second peripheral (deep) compartments, in that order. Clearance values for distribution between compartments are given by CLD2 (central-to-shallow peripheral) and CLD3 (central-to-deep peripheral). For the CAR-T product indicator, a value of 1 corresponds to Axi-cel, while 2 corresponds to Tisa-cel.

Model evaluation

According to the pcVPC, the observed median and the 2.5th and 97.5th percentiles fell within the model's simulated prediction range **(Figure 3).**

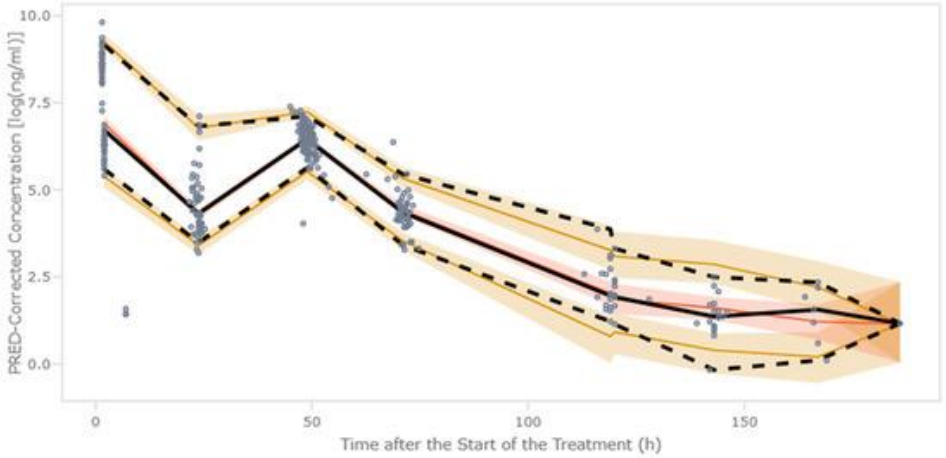

Figure 3. Prediction-corrected visual predictive check (pcVPC) results. For each time interval, the colored bands indicate the 95% prediction intervals derived from the 2.5th and 97.5th percentiles calculated across 1,000 simulated datasets. The solid line traces the median of the 1,000 50th percentiles, while the dashed line represents the corresponding median from the observed raw data. Open circles denote prediction-corrected observations.

Figure 4 illustrates how the selected covariates influenced fludarabine serum concentration over time. For each continuous variable (body weight and eGFR), typical concentration–time curves were generated corresponding to the 10th, 50th, and 90th percentiles observed in the patient population. Regarding the categorical CAR-T construct variable, typical profiles were generated separately for axicabtagene ciloleucel and tisagenlecleucel. Across all simulated scenarios and patients, the administered dose was kept unchanged.

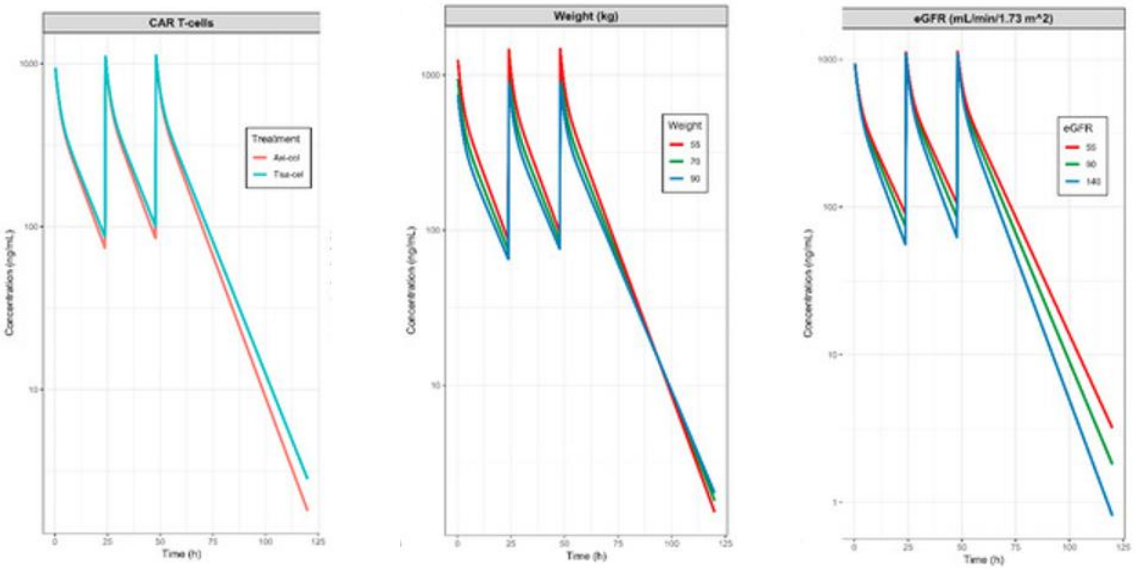

a) b) c)

Figure 4. Influence of the selected covariates on fludarabine's typical pharmacokinetic behavior. The a, c) panels employed the median weight distribution; the a, b) panels used the median eGFR; and the b, c) panels applied the axicel CAR-T construct.

The initial simulation distinguished between the two LDC dosing schedules based on the CAR T cell product provided, with protocols requiring higher doses associated with lower observed concentrations. A stratified analysis by weight revealed that under fixed dosing, individuals with lower body weight initially reached higher concentrations, yet this same subgroup showed the lowest terminal levels over extended time. Furthermore, eGFR exerted a strong impact on drug plasma levels, with concentration trajectories separating immediately after dosing and culminating in a fivefold disparity between the 10th and 90th percentiles at the final simulated time points.

While this observation aligns with diminished renal elimination, the precise magnitude should be interpreted cautiously, considering residual variability and model precision. Patients presenting with reduced eGFR exhibited progressive fludarabine accumulation alongside delayed clearance.

Using nonlinear mixed-effects analysis, we sought to develop a dedicated population pharmacokinetic model to improve fludarabine-based lymphodepleting chemotherapy (LDC) for individuals with relapsed/refractory large B-cell lymphoma receiving CD19-targeted CAR T therapy. A three-compartment configuration with first-order elimination provided the best fit to fludarabine PK data. Statistically significant covariate effects were observed for body weight, renal status, and the specific CAR-T product administered. As far as we are aware, this is the first pharmacokinetic model built exclusively from data collected in patients undergoing CAR T-cell treatment, with the explicit goal of describing fludarabine disposition in this population.

Previous popPK models characterizing fludarabine have mainly focused on HSCT populations, often involving either adult-only or combined pediatric-adult groups [14, 29, 30]. In most such studies, body size and renal function were identified as the principal determinants of fludarabine clearance, reflecting both the predominantly renal excretion of F-ara-A and the tight linkage between drug clearance and creatinine clearance [11, 12]. A three-compartment model developed by Langenhorst *et al*. [14] included renal function as a major driver of fludarabine CL. Observing lower clearance in subjects with eGFR values under 120 mL/min/1.73 m², those investigators proposed a carboplatin-like dosing strategy to facilitate more individualized therapy. By contrast, Sanghavi and Ivaturi [29, 30] found that two-compartment models adequately captured their data, likely due to variations across study cohorts and blood sampling protocols. However, because these earlier models originated from transplant contexts—typically featuring younger patients with relatively preserved kidney function—they may not adequately represent the clinical reality of CAR-T recipients, who are often older, extensively pretreated, and prone to variable renal function. Beyond these pharmacokinetic factors, the characteristics and intensity of lymphodepletion conditioning have been linked to subsequent CAR T cell expansion and clinical outcomes. Among those with aggressive NHL, better progression-free survival was observed in patients who developed a favorable cytokine profile after high-intensity conditioning compared with those who had similar depletion intensity but lacked such cytokine modulation [31]. Hence, a CAR-T-tailored popPK model is needed to optimize lymphodepletion and reduce between-subject variability in this patient group [29, 30].

Published population pharmacokinetic studies report total fludarabine clearance in adults or mixed age groups ranging from about 5 to 7 L/h/70 kg. A lower value (3.98 L/h/70 kg) was obtained from Langenhorst's three-compartment work. Sanghavi's analysis confirmed that both eGFR and weight influence clearance in grown-up patients, yet a noticeable amount of unexplained scatter remained after covariate inclusion. A more recent three-compartment investigation [32] broke down fludarabine elimination into renal and non-renal components using unbound concentrations. That study again highlighted eGFR and weight as relevant predictors but still reported high levels of both interindividual and inter-occasion variability, indicating that additional hidden factors drive fludarabine disposition. Taking a typical patient weighing 70 kg with a median eGFR of 96 mL/min, the projected clearance equaled 6.1 L/h for those on axi-cel and 5.6 L/h for the tisa-cel group. These figures fall within the adult ranges from prior popPK publications.

In our work, allometric normalization based on body weight proved best for handling size differences across individuals. Once eGFR entered the model, no age-related effects persisted beyond those accounted for by body dimensions. Because fludarabine undergoes extensive renal elimination via both filtration and active secretion, adding creatinine clearance as a covariate was biologically logical and matched earlier reports. Our calculated volumes of distribution were 41.2 L for the central compartment, 14.5 L for the shallow peripheral space, and 10.8 L for the deep peripheral compartment. Distribution volume depends on plasma protein binding and total body water, the latter accounting for 60%–75% of total body weight [33]. Other fludarabine population models have produced V1 estimates of 9.6-39 L/70 kg, V2 estimates of 8-20 L/70 kg, and V3 estimates of 16-50 L/70 kg, lending biological support to our own results [14, 32]. As for the CAR-T product type covariate, its influence may stem from complex, multidimensional biological distinctions between the patient subsets treated with each construct. Such distinctions could involve tumor biology, prior lines of therapy, disease burden, or individual immunological and metabolic traits. Even though adding the CAR-T construct significantly reduced the objective function value, the almost negligible change in typical parameter estimates, together with the diagnostic plot behavior, suggests this effect is probably not clinically relevant. It might simply reflect unmeasured confounding or other case-specific factors. These observations highlight why personalized fludarabine dosing matters—to boost the expansion and persistence of engineered cells and thereby enhance the effectiveness of CAR-T therapy.

Several limitations of this work should be acknowledged. First, the analysis was based on a modest sample size and a relatively brief enrollment period of 19 months. Furthermore, restricted sampling at the 7-hour post-fludarabine time point—when the β/γ transition occurs—may have compromised the precision of our V3 and CLD3 estimates. This limitation arose because many patients received lymphodepleting chemotherapy in an outpatient setting, complicating specimen collection. Nevertheless, the cohort still contributed over 340 serial samples from individuals with large B-cell lymphoma receiving commercially available CAR-T products.

Additionally, while the sampling schedule followed a limited sampling strategy originally validated in hematopoietic stem cell transplant populations, its application to CAR-T recipients may entail minor drawbacks. Second, as a single-center investigation, our findings may not fully reflect the diversity of clinical practices and patient characteristics observed across institutions. Third, pharmacogenetic data were not available; specifically, we did not assess the rs2295890 variant described by Mohanan *et al*. [20], which has been linked to lower FaraA plasma levels in wild-type individuals. Although including this genetic factor might enhance the model, omitting it is unlikely to undermine its overall validity. Fourth, stepwise covariate selection carries an inherent risk of Type I error, meaning some covariate-parameter relationships might emerge by chance. While this represents a recognized limitation of the approach, the model's overall predictive capability should remain dependable. Finally, although this study primarily characterizes fludarabine pharmacokinetics, the lack of an exposure–response evaluation (linking area under the curve to neurotoxicity, cytokine release syndrome, or CAR-T expansion) restricts its immediate clinical translation. Larger, multi-center, prospective investigations will be necessary to confirm the predictive value of this model and its potential role in guiding individualized fludarabine dosing within CAR-T therapy.

This study also offers several notable strengths. As far as we are aware, this represents the first prospectively developed population pharmacokinetic model specifically designed for patients receiving CAR-T cell therapy. Currently, the fludarabine prescribing information recommends a dose reduction of up to 50% only when eGFR drops below 70 mL/min/1.73 m². Nevertheless, Langenhorst and colleagues found that fludarabine clearance already declines in patients with eGFR below 120 mL/min/1.73 m² [14]. Given that chronic kidney disease occurs frequently among cancer patients undergoing active treatment—with roughly 10%–20% of them having stage III or worse CKD (eGFR < 60 mL/min/1.73 m²) [34]—our popPK model could prove valuable for achieving precise dose customization in this subgroup. Our findings enable the use of population pharmacokinetic modeling to tailor lymphodepletion to each patient. Employing a dedicated predictive model to define an optimal fludarabine exposure range holds promise for improving clinical outcomes in this large B-cell lymphoma population, where 40–50% of patients fail to achieve sustained long-term survival [35].

Furthermore, because fludarabine-based lymphodepleting regimens are widely employed across multiple CAR-T indications and product types, this personalized strategy could benefit a wide array of patients with both malignant and non-malignant diseases [35, 36]. That said, real-time approaches requiring narrow intervention windows—such as the one proposed here—come with inherent financial and logistical hurdles that may restrict their widespread adoption. The blood sampling protocol and the accompanying model were designed to facilitate the incorporation of therapeutic drug monitoring into everyday clinical workflows, thereby enhancing accessibility to individualized dosing. Upcoming investigations will clarify the extent to which pharmacokinetic-guided strategies can be implemented effectively in routine practice.

Conclusion

A dedicated population pharmacokinetic model was developed via nonlinear mixed-effects analysis for individuals with relapsed/refractory large B-cell lymphoma who received fludarabine-based lymphodepletion before CAR T therapy to optimize exposure to fludarabine. A three-compartment structure incorporating first-order elimination provided the best description of the observed data. Actual body weight, renal function, and the specific CAR-T product administered emerged as statistically meaningful covariates. By improving fludarabine exposure during the lymphodepletion phase, this model represents a step forward toward individualized dosing strategies and may serve as a future tool to enhance CAR-T cell effectiveness.

Acknowledgments: The authors express their gratitude to Iosune Baraibar for her help with manuscript preparation. We also wish to thank every patient who took part in this project and contributed to sample collection.

This research was carried out as part of the Department of Medicine's activities at the Universitat Autònoma de Barcelona.

Conflict of Interest: G.I. has consulting agreements with Autolus, BMS, Kite/Gilead, Miltenyi, and Regeneron. He also receives honoraria from AbbVie, AstraZeneca, BMS, Gilead/Kite, Miltenyi, Sobi, Roche, and Lilly. Travel support has been provided by AbbVie, AstraZeneca, Gilead/Kite, Miltenyi, and Roche. M.J.C. serves as a consultant or receives honoraria from Boehringer, Daiichi Sankyo, GSK, Janssen, Menarini, Novartis, Regeneron, Roche, Seagen Spain SLU, and Takeda. Travel grants have been given by Daiichi Sankyo, Ipsen, Janssen, Roche, and Servier. C.V. has participated as a paid speaker and has received accommodation and educational support from Bayer Hispania S.L., Janssen Cilag S.A., Novartis Farmaceutica S.A., and Grifols S.A. P.B. has consulting roles with AstraZeneca, Autolus, BMS, Gilead/Kite, Pfizer, and Novartis. Honoraria are received from Amgen, AstraZeneca, BMS, Gilead/Kite, Novartis, and Pfizer. Travel funding is provided by AstraZeneca, Gilead/Kite, Novartis, and Pfizer. No other authors declare any competing interests.

Financial Support: The present study was funded by the Instituto de Salud Carlos III under awards PI21/00197 and INT23/00072.

Ethics Statement: The Clinical Research Ethics Committee at HUVH approved this study. The protocol identifier is IP17/2020-PR(AG)682/2020, and the approval date was December 1, 2020.
Every participant included in the study provided written informed consent.

References

1. Sehn LH, Salles G. Diffuse large B-cell lymphoma. N Engl J Med. 2021;384:842-58.
2. Dwyer M. NCCN Clinical Practice Guidelines in Oncology (NCCN Guidelines®) B-Cell Lymphomas. NCCN Guidelines for Patients®. 2025. Available from: NCCN Guidelines for Patients (cited 2025 Nov 17).
3. CHMP. Yescarta 0.4-2×10^8 cells dispersion for infusion: Summary of product characteristics (SmPC). Available from: EMA Yescarta Product Information (cited 2024 Nov 25).
4. CHMP. Kymriah 1.2×10^6-6×10^8 cells dispersion for infusion: Summary of product characteristics (SmPC). Available from: EMA Kymriah Product Information (cited 2024 Nov 25).
5. CHMP. Breyanzi 1.1-70×10^6 cells dispersion for infusion: Summary of product characteristics (SmPC). Available from: Breyanzi Product Information PDF (cited 2025 Sep 10).
6. Ninomiya S, Narala N, Huye L, Yagyu S, Savoldo B, Dotti G, et al. Tumor indoleamine 2,3-dioxygenase (IDO) inhibits CD19-CAR T cells and is downregulated by lymphodepleting drugs. Blood. 2015;125:3905-16.
7. Turtle CJ, Hanafi LA, Berger C, Hudecek M, Pender B, Robinson E, et al. Immunotherapy of non-Hodgkin's lymphoma with a defined ratio of CD8+ and CD4+ CD19-specific chimeric antigen receptor-modified T cells. Sci Transl Med. 2016;8:355ra116.
8. Canelo-Vilaseca M, Sabbah M, Di Blasi R, Cristinelli C, Sureda A, Caillat-Zucman S, et al. Lymphodepletion chemotherapy in chimeric antigen receptor-engineered T (CAR-T) cell therapy in lymphoma. Bone Marrow Transplant. 2025;60:559-67.
9. Gandhi V, Plunkett W. Cellular and clinical pharmacology of fludarabine. Clin Pharmacokinet. 2002;41:93-103.
10. Bonin M, Pursche S, Bergeman T, Leopold T, Illmer T, Ehninger G, et al. F-ara-A pharmacokinetics during reduced-intensity conditioning therapy with fludarabine and busulfan. Bone Marrow Transplant. 2007;39:201-6.
11. Lichtman SM, Etcubanas E, Budman DR, Eisenberg P, Zervos G, D'Amico P, et al. The pharmacokinetics and pharmacodynamics of fludarabine phosphate in patients with renal impairment: A prospective dose adjustment study. Cancer Investig. 2002;20:904-13.
12. Long-Boyle JR, Green KG, Brunstein CG, Cao Q, Rogosheske J, Weisdorf DJ, et al. High fludarabine exposure and relationship with treatment-related mortality after nonmyeloablative hematopoietic cell transplantation. Bone Marrow Transplant. 2011;46:20-6.

13. Langenhorst JB, van Kesteren C, van Maarseveen EM, Dorlo TPC, Nierkens S, Lindemans CA, et al. Fludarabine exposure in the conditioning prior to allogeneic hematopoietic cell transplantation predicts outcomes. Blood Adv. 2019;3:2179-87.
14. Langenhorst JB, Dorlo TPC, van Maarseveen EM, Nierkens S, Kuball J, Boelens JJ, et al. Population pharmacokinetics of fludarabine in children and adults during conditioning prior to allogeneic hematopoietic cell transplantation. Clin Pharmacokinet. 2019;58:627-37.
15. Dekker L, Calkoen FG, Jiang Y, Blok H, Veldkamp SR, De Koning CCH, et al. Fludarabine exposure predicts outcome after CD19 CAR T-cell therapy in children and young adults with acute leukemia. Blood Adv. 2022;6:1969-76.
16. Fabrizio VA, Boelens JJ, Mauguen A, Baggott C, Prabhu S, Egeler E, et al. Optimal fludarabine lymphodepletion is associated with improved outcomes after CAR T-cell therapy. Blood Adv. 2022;6:1961-8.
17. Fludarabine 25 mg/mL concentrate for solution for injection. Summary of product characteristics (SmPC). 2025. Available from: Fludarabine SmPC (cited 2025 Jan 13).
18. Cockcroft DW, Gault H. Prediction of creatinine clearance from serum creatinine. Nephron. 1976;16:31-41.
19. Sociedad Española de Nefrología Renal Function Calculator. Calculadora de Función Renal. cited 2022 May 17.
20. Mohanan E, Panetta JC, Lakshmi KM, Edison ES, Korula A, Fouzia NA, et al. Population pharmacokinetics of fludarabine in patients with aplastic anemia and Fanconi anemia undergoing allogeneic hematopoietic stem cell transplantation. Bone Marrow Transplant. 2017;52:977-83.
21. EMA ICH M10 Bioanalytical Method Validation Guideline. ICH M10 on bioanalytical method validation-scientific guideline. cited 2025 Nov 10.
22. Beal SL, Sheiner LB, Boeckmann A. NONMEM 7.4.0 users guides. Ellicott City (MD): Icon Development Solutions; 2009. p. 1989-2009.
23. Lindbom L, Ribbing J, Jonsson EN. Perl-speaks-NONMEM (PsN)-A Perl module for NONMEM related programming. Comput Methods Programs Biomed. 2004;75:85-94.
24. R Core Team. R: A language and environment for statistical computing. Vienna: R Foundation for Statistical Computing; 2021. Available from: R Project for Statistical Computing (cited 2022 May 17).
25. Pirana, version 11.1. Princeton (NJ): Certara USA, Inc.; 2023.
26. Anderson BJ, Holford NHG. Mechanistic basis of using body size and maturation to predict clearance in humans. Drug Metab Pharmacokinet. 2009;24:25-36.
27. Bergstrand M, Hooker AC, Wallin JE, Karlsson MO. Prediction-corrected visual predictive checks for diagnosing nonlinear mixed-effects models. AAPS J. 2011;13:143-51.
28. Largajolli A, Bertoldo A, Campioni M, Cobelli C. Visual predictive check in models with time-varying input function. AAPS J. 2015;17:1455-63.
29. Ivaturi V, Dvorak CC, Chan D, Liu T, Cowan MJ, Wahlstrom J, et al. Pharmacokinetics and model-based dosing to optimize fludarabine therapy in pediatric hematopoietic cell transplant recipients. Biol Blood Marrow Transplant. 2017;23:1701-13.
30. Sanghavi K, Wiseman A, Kirstein MN, Cao Q, Brundage R, Jensen K, et al. Personalized fludarabine dosing to reduce nonrelapse mortality in hematopoietic stem-cell transplant recipients receiving reduced intensity conditioning. Transl Res. 2016;175:103-15.e4.
31. Hirayama AV, Gauthier J, Hay KA, Voutsinas JM, Wu Q, Gooley T, et al. The response to lymphodepletion impacts PFS in patients with aggressive non-Hodgkin lymphoma treated with CD19 CAR T cells. Blood. 2019;133:1876-87.
32. Nath CE, Rosser SPA, Nath KK, Chung J, Larsen S, Gibson J, et al. The impact of age and renal function on the pharmacokinetics and protein binding characteristics of fludarabine in paediatric and adult patients undergoing allogeneic haematopoietic stem cell transplantation conditioning. Eur J Clin Pharmacol. 2024;80:1967-87.
33. Wallace G, Ramsden D, Grant M. General principles of drug disposition. In: Encyclopedia of Drug Metabolism and Interactions. Hoboken (NJ): John Wiley & Sons Inc.; 2012.
34. Ubukata M, Hara M, Nishizawa Y, Fujii T, Nitta K, Ohta A. Prevalence and mortality of chronic kidney disease in lymphoma patients: A large retrospective cohort study. Medicine (Baltimore). 2018;97:e9615.

35. Neelapu SS, Locke FL, Bartlett NL, Lekakis LJ, Miklos DB, Jacobson CA, et al. Axicabtagene ciloleucel CAR T-cell therapy in refractory large B-cell lymphoma. N Engl J Med. 2017;377:2531-44.
36. Müller F, Taubmann J, Bucci L, Wilhelm A, Bergmann C, Völkl S, et al. CD19 CAR T-cell therapy in autoimmune disease-A case series with follow-up. N Engl J Med. 2024;390:687-700.